A MULTIPLE-BEAM SCANNING CIRCULAR ARRAY

By GEORGE G. CHADWICK, JOHN C. GLASS, and JEROME E. HILL
Engineering Deportment
Radiation Systems Inc.
Alexandria, Virginia

Summary The geometry of the cylindrical array has always been appealing to system designers because of its ability to provide 360° of coverage. A technique will be discussed which allows a cylindrical array to provide high-resolution coverage over 360° of azimuth angle. When used as a scanning array, a beam may be swept through 360° by using any of the numerous techniques available for scanning a linear array. When used to provide multiple beams, an array of N elements is excited by N isolated inputs. Each input corresponds to a beam in a selected direction; all of the N beams being disposed uniformly over 360° of azimuth angle. In both the instance of the scanning array and the multiple-beam array, the resolution achieved is comparable to that available from a planar aperture of the same height and with a length equal to that of the cylinder diameter. The theory of operation for the cylindrical array is discussed in abridged form. Data are also presented for experimental four-, eight-, and sixteen-element cylindrical arrays.

Introduction An RSi conceived technique will be discussed which reduces the problem of processing antenna elements of cylindrical arrays to one analogous to the element processing used in linear arrays. This equating of the array processes allows all of the techniques developed for linear arrays to be directly applied to cylindrical arrays. A partial listing of these processing techniques would include the synthesis of any desired far-field radiation patterns commensurate with aperture size, the scanning of the synthesized patterns, or the multiple beaming of the synthesized patterns. Hence, the cylindrical array may be used to provide steerable or multiple beams over 360° of azimuth angle.

In the conventional linear array, each element is controlled in amplitude and phase to achieve a given result. In the cylindrical array, the outputs of each element of an array, having N elements, are processed by a network having N inputs. Each input excites all of the N-array elements with equal amplitudes, but with differing phase excitations. These phase excitations are progressive. The increments of phase progression increase from one processing port to the next. The resulting far-field patterns for each of these modes are nearly omnidirectional for the instance where the phase progression between the

elements is not large. As the interelement phase progression increases with increasing mode number, the omnidirectivity of the mode deteriorates considerably. When the highest order mode is used, the phase progression between elements is 180°. This type of phase excitation generates an N-lobed amplitude pattern which, because of its special nature, is only useful for multiple-beam applications. The far-field phase pattern of the remaining modes is not uniform with azimuth angle but will vary from zero to ±(N - 2)Ø/2 degrees (where Ø is the azimuth angle), depending on which input port is excited. The mathematical form of the pseudo omnidirectional patterns, generated by these remaining (N - 1) input ports, differs from the mathematical form of the individual elements of a linear array only in the definition of the argument. Since the patterns generated by the inputs of the circular array processing network are of the same form as those used for a linear array, it follows that they may, in turn, be processed by any of the myriad techniques used to process a linear array.

It is important to distinguish between the individual terms used in both cases. In the linear array, the elemental terms represent the contribution of a single radiator in the array. In the cylindrical array the equivalent elemental terms each represent the equiamplitude progressive phase excitation of all N elements. The distinction between the cylindrical array terms, or modes, is simply the incremental phase difference between each of the N elements.

It should be noted that this paper represents an abridged version of the theoretical and experimental work which has been conducted on the cylindrical array technique. A number of technical reports, prepared by the authors, are available[1,2,3)] which completely detail the theory of operation of the cylindrical array technique and experiments performed to verify the technique.

The Basic Concept Figure 1 is a sketch depicting N radiating elements arranged to form a ring in the horizon plane. The spacial orientation of the array, and the physical array parameters denoted in this figure will be used throughout the remainder of the discussion. The radiation patterns realizable from this type of array may be represented in complex Fourier form as

$$E(\theta,\phi) = A_o(\theta) + A_1(\theta)e^{j\phi} + A_2(\theta)e^{j2\phi} \text{ --- } A_N(\theta)e^{jN\phi} \tag{1}$$

or more simply in the summation form,

$$E(\theta,\phi) = \sum_{n=0}^{n=N-1} A_n e^{jn\phi} . \tag{2}$$

In the earlier applications, most investigators were only interested in exciting the A_o term to achieve an equiphase, equiamplitude distribution of radiated energy in the Ø plane.

The imperfections in these patterns, both in phase and amplitude were generally minimized. These imperfections, represented by the remainder of the Fourier terms, generally increased with frequency, thereby limiting the range of frequencies over which a given maximum level of imperfection could be achieved. Later efforts were concerned with the generation of single-lobed patterns. These patterns were indirectly realized by the judicious control of the coefficients An- It should be noted, however, that the design procedure was not generally synthesized directly from the Fourier series of equation (1). Early beam-forming methods modified the element phases with line length devices to form a plane wave front and then the element excitation was varied to achieve a given beam shape. Nonetheless it can be shown that equivalent results could have been achieved by controlling the amplitude coefficients of equation (1).

The idea of synthesizing any beam from a circular array that could be synthesized from a linear array first germinated when the similarity of their basic format was recognized. The general expression for a linear array of N elements may be written directly as

$$E'(\phi) = \sum_{n=0}^{n=N-1} A_n e^{jnu} \qquad (3)$$

where: $E'(\phi)$ = the array factor of an array of N linear elements
N = the number of elements
A_n = the n^{th} amplitude excitation coefficient
u = $k S \cos \phi$
k = $2\pi/\lambda$
S = element spacing.

If the comparison between (1) and (3) is limited to one plane, it becomes apparent that the only significant distinction between the two equations is the form of the argument. In the instance of the ring array, the argument is simply ∅, the azimuth angle. However, in the case of the linear array, the argument is u (= k S cos ∅). Except for limits then, it follows that the same degree of freedom exists in both cases for synthesizing patterns. The basic problem heretofore with the circular array has been the absence of a technique which would allow separable excitation of the individual terms of equation (1). In the linear array this separable excitation is a simple matter since each term represents the contribution of a single element. In the circular array, the complex spacial arrangement does not allow the individual elements to represent the individual terms of equation (1). However, if a method were generated for separately and independently exciting each of the terms of (1), it would follow that the problem of synthesizing beams from a circular array would be no more difficult than synthesizing beams from a linear array.

It will be shown later that the individual terms, or expressions of equation (1). may be separably excited. However, in the general case, no term can be excited without some content of the remaining terms existing. To examine the degree of imperfection in any

given mode, it is necessary to theoretically analyze the phase and amplitude characteristics of a given mode.

The Fourier synthesis of patterns from circular arrays has been the object of considerable study during the course of the last few years. A synthesis technique utilized by Taylor [4] traced the steps from the required pattern to the element coefficients, and an intermediate expression for the pattern involving a complex Fourier series was formulated. Although Taylor did not directly state that there was a limit on the allowable phase progression, he did indicate that the array size very sharply limits the highest order term that can be realized in the Fourier Series. The result is that the progressive phase excitation radiates the desired terms predominantly with higher order terms entering as unwanted perturbations. The magnitude of these perturbations can be evaluated by the method of TaShing [5] for in-phase arrays. When this expression is modified to take into account the progressive phase of the excitation, the following equation is obtained for the p^{th} term:

$$E_p(\theta, \phi) = N \left\{ \sum_{n=o}^{\infty} A_n^{(p-n)} \frac{d^n}{dz^n} \left[J_p(Z) \right] e^{jp\phi} \right\}$$

$$+ N \sum_{x=-\infty}^{\infty}{}' \left\{ \sum_{n=o}^{\infty} A_n j^{(p-n-N_x)} \frac{d^n}{dz^n} \left[J_{(p-N_x)} \right] e^{j(p-N_x)\phi} \right\} \qquad (4)$$

where:

$E_p(\phi, 0)$	is the relative pattern of the p^{th} mode
J_p	is a bessel function of order p
Z	$= (2\pi r/\lambda) \sin\theta$
N	= number of elements
n	is an integer

The prime on the summation indicates that the term x = 0 is excluded. The element pattern, which has been integrated into the above expression, is expressed as a Fourier series of the form,

$$E_e(\phi, \theta) = \sum_{n=-\infty}^{n=+\infty} A_n(\theta) e^{jn\phi} \qquad (5)$$

where the amplitude coefficient A_n is a function of elevation angle.

The first bracketed expression of equation (4) is the desired far-field characteristic. The second part of the equation represents the unwanted residuals which cause undesired amplitude and phase distortion of the desired mode. The first section has an amplitude which is independent of azimuth angle, and has a phase characteristic which increases linearly with increasing azimuth angles. A significant factor is the relative phase of the expression as a function of p, the mode number. The j term is raised to the (p-n) power, so that for any two given modes, a fixed-phase differential will occur.

Thus, in order to correlate the modes properly, a fixed-phase correction will have to be inserted in each port. The magnitude of this fixed-phase difference will be a function of the element patterns and spacings. If the element patterns remain reasonably constant with frequency, the fixed-phase shift will, in turn, vary little with frequency; thereby allowing for the possibility of broadband operation.

It is interesting to note that the maximum value of p is N/2 which corresponds to a 180-degree phase shift from element to element. For this value of p, it is impossible to excite an $e^{j(N/2)\emptyset}$ term without also exciting a complementary residual of $e^{-j(N/2)\emptyset}$. The sum of these two terms is equal to cos N/2 $\emptyset$ (ignoring higher order residuals), indicating that the far-field pattern has nulls and maxima equal in number to the value of N. Another factor of interest is that the pattern mode with the next highest residual content is $E_{(N/2)-1}$ ($\emptyset$), which has an associated perturbation of order -(N/2 + 1). It is here that the cutoff effect can be seen in terms of the Bessel function of argument z. With an increase in the order of p, Jp (z) increases and, since Bessel functions decay rapidly for values of the argument less than the order, z must have a larger value to avoid cutoff. It is also easy to see why the $E_o(\emptyset)$ pattern (in-phase array) has the optimum omnidirectivity because its first residual term has the highest order ------±N.

The mode characteristics, as represented by equation (4), were tabulated on an IBM 7090 computer for arrays of 8, 16, 32, and 48 elements. These mode characteristics were tabulated for theoretical element patterns of the form

$$E(\emptyset) = \cos^r(\emptyset) \tag{6}$$

where r was made to range from 0 to 16. Computed data were also tabulated for experimentally measured element patterns in the instance of both the 8 and 16 element arrays. In all of the above instances, an element spacing range from 0.25 to 0.75λ was investigated. These tabulations are much too extensive for this paper, but may be found in references 1 through 3. The computed data of Figure 2 is exemplary of the curves obtained from the expression of equation (4). The curves represent the tabulated data for the instance where r = 16 and where N, the number of elements, is also equal to 16. The graph of Figure 2(a) represents the minimum-to-maximum voltage ratio (ρ) in the azimuth plane as a function of mode number. The curve of Figure 2(b) represents the phase deviation from the desired phase progression, as a function of mode number. The mode number is of the form 0m or m0, where m represents the number of 2π phase progressions about the array periphery. In the former instance, the notation indicates that the progression is clockwise, as viewed from the top of the array; in the latter instance, the notation indicates that the phase progression is counterclockwise. It should be noted that, while the curves of Figure 2 are shown as continuum, in actual fact they are only valid for integral values of p. Generally, all of the data computed from equation (4) had

the same format as that of Figure 2, differing only in detail. In all instances, the amplitude and phase deviations increase with increasing mode number, increasing element spacing, and increasing element beamwidth.

A typical set of voltage amplitude patterns is plotted in Figure 3 for the conditions assumed in Figure 2, and for the case where the spacing is equal to 0.5λ. The plot is shown over the range from $\emptyset = 0$ to $\emptyset = 1.6$ radians. The full range of $\emptyset$ is not included, since the functions are periodic over increments of $\pi/8$.

The definition of the individual mode patterns represents an intermediate step for the computation of the eventual far-field patterns which will be formed by judiciously combining the modes. While the data of Figures 2 and 3, and the expression from which the data were evolved is rigorous, it does not allow for simple programming even by computer processing standards. Since the rigorous expression represents an unwarranted amount of programming, it is desirable to seek an expression which would approximate the computed mode patterns, but which would be more amenable to simple programming. The general expression for this approximation could then be summed for eventual synthesis by further processing networks. This be written as:

$$E(\emptyset, p) = e^{j\delta p}\left[e^{j\emptyset p} + kp\, e^{j\left[\emptyset p\,(1 - 48/|p|) + py_p/|p|\right]}\right] \cdot \left[1 + kp\right]^{-1} \qquad (6)$$

where: δp is the base reference phase for each mode
yp is the phase parameter which defines the position of the first amplitude minimum relative to element number 1 ($n = 1$)
kp is the amplitude of the perturbing higher order mode

The value of kp may be defined or derived from the simple relationship:

$$kp = (1 - \rho)/(1 + \rho), \qquad (7)$$

where ρ is the ordinate of Figure 2. The position of the first pattern minima for each mode, relative to element number 1, may be taken directly from the earlier described computed data. The use of this latter parameter now insures that the amplitude deviations are not only correct, but are also properly oriented. In reference 3 a number of test cases utilizing an expression similar to equation 8 were analyzed. In all instances the deviations between the patterns predicted by the computer, using the approximate expression, agreed within 1.5 per cent of the data obtained using the rigorous expression of equation (4).

The approximating expression of equation (6) may now be utilized to examine the mode outputs and compare them with the output of a single element in a conventional linear

array. If the value of ρ in expression (7) approaches 0, then the equation simplifies to:

$$E(\emptyset, p)_{kp} \xrightarrow{=} 0 \quad \delta p \quad e^{j\emptyset p} \tag{8}$$

This expression is reasonably valid for the lower order mode numbers and for close element spacings. The striking resemblance between the mode pattern of equation (8) and the element contributions in a linear array may be observed by comparison with equation (3). A comparison of equation (3) and equation (8) will indicate that the only significant difference between the two, outside of the element factor, is the argument. In the instance of the circular array, the argument contains only the parameter ∅. In the instance of the linear array, the argument involves the element spacing and sin ∅. Hence, while the circular array expression is not a function of frequency, the linear array term is.

In actual fact, of course, the cylindrical array term is not frequency insensitive. The fundamental, although it does not contain a frequency component, has a perturbing higher-order mode which increases in magnitude with increasing frequency. The question now arises as to the effect of the perturbing terms particularly for the higher-order modes. The number of elements, or equivalent elements, for the circular array could be viewed as being equal to twice the number of the mode terminals. Half of the outputs would consist of the fundamental terms, and the remaining half would consist of the higher-order terms. However, these higher-order terms are inseparable from the fundamental terms, and whatever excitation applies to the fundamental of a given mode will also apply to the higher-order term. Fortunately, these higher-order terms for most of the modes are highly attenuated and rather random in phase and amplitude. Experience with the synthesis of modes containing perturbing terms has proved that the higher-order terms tend to average, having only a secondary effect on the characteristics of the synthesized beam. The general effect is to slightly distort the main beam with a general improvement in the expected sidelobe level. For example, in reference 3, a synthesis program was established which combined the mode terminals with a Tchebysheff distribution for -25 db sidelobe levels. The performance of the array was theoretically examined over a 50 per cent bandwidth. It was found that the sidelobes were less than -26 db, but that the beam tended to have shoulders which caused a variation in the beamwidth.

Some method of exciting all the terms of equation (1) separately and simultaneously is fundamental to the concept of the cylindrical array. The feeding network must excite all of the array elements with equal amplitude for all N input ports. However, the phase progression must vary from one input to another. An N port multiple-beam matrix has this capability. The manner in which this matrix functions has been described in the literature [6, 7,8. 9)], and hence will not be repeated here.

General Block Diagram Configurations Figure 4 contains the generalized block diagrams for a scanning cylindrical array and for a multiplebeam cylindrical array. In both instances, the radiating structure is a ring of N elements of arbitrary elevation configuration. The outputs of these N element arrays are processed by an N input - N output matrix. It is these outputs which have the format that is closely related to the format of the expression for a single element in a linear array. The mathematical expression for each of these outputs is given rigorously by equation (4) or by the approximate expression of equation (8). The base phasors are necessary to adjust all outputs to the same phase reference. This base phase correction may be derived from the rigorous expression of equation (4).

When the cylindrical array technique is utilized to form a scanning beam, a conventional matched power divider may be utilized, with in-line phase shifters providing the needed scan parameter. The amplitude coefficients for each of the mode inputs may be controlled to synthesize any desired pattern, by simply controlling the power distribution at the output of the combiner. Note, that in the instance of the scanning array the last term, which generates the N-lobed mode pattern, is not used.

The block diagram of the multiple-beam cylindrical array is similar to that of the scanning array, except that the combiner and the scan control phase shifters have been replaced by a multiple-beam matrix of the same format as the mode-forming matrix. In this latter instance, the last mode can be utilized if the beams are made to lie in the directions of the elements. The outputs of the multiple-beam matrix are equal in number to the number of elements in the array. The multiple-beam technique generates sidelobes which are theoretically 13 db below the main beam amplitudes. Amplitude tapering techniques presently used in linear arrays for modifying the multiple-beam uniform distribution, can be applied directly to the cylindrical array 1).

A detailed analysis of the far-field patterns of the scanning and multiplebeam circular arrays is contained in reference 1, but is beyond the scope of this discussion. However, it should be noted that if the element spacing is equal to 0.5λ , the resolution obtainable with the circular array is equivalent to that of a linear array having the same element spacing and with a length equal to the diameter of the cylindrical array. The following paragraphs will now detail some of the experimental data obtained With arrays of varying numbers of elements.

An Experimental Four-element Multiple-beam Cylindrical Array Figure 5 is a photograph of an experimental four-element cylindrical array. In this instance, monopole elements were utilized as a matter of convenience. The two strip transmission line matrices, shown below the array, represent the mode-forming and the beam-forming matrices. The mode patterns obtained for each of the four modes of the array are shown

in the upper half of Figure 6. The sketch in the lower half of Figure 6 depicts the far-field pattern data obtained at each of the output ports of the final multiple-beam matrix. Note that the pattern format and beam crossovers are closely related to those obtainable from a linear array with the exception that the range of azimuth angle is now 360°.

An Experimental 4 x 8-Element Circular Array Figure 7 is a photograph of a 4 x 8 element circular array. This array provides eight beams in azimuth at each of four elevation stations, for a total of 32 beams. The total elevation coverage is approximately ±45°. Figure 8 represents the patterns obtained at two elevation stations for this array. Note that the sidelobe level deteriorates somewhat for the upper elevation station. This eterioration in the sidelobe levels is theoretically predictable and can be reduced by proper selection of the element pattern characteristics.

An Experimental Sixteen-element Circular Array Figure 9 is a photograph of an experimental 16-element circular array. In this instance, a total of 16 beams are formed, the characteristics of which are shown in the pattern of Figure 10.

Conclusions The preceding discussion has outlined a technique for processing a cylindrical in such a manner that passive techniques may be utilized to provide reciprocal coverage over 360° of azimuth. The cornerstone of the technique is a mode-forming matrix which translates the outputs of the cylindrical array into a format which is analogous to the mathematical format of a single-element contribution in a linear array. The theory of operation of the technique was presented in abridged form. It was shown that the characteristics of the individual modes can be predicted and that an approximating expression can be generated which is valid for each of these modes. The desired far-field patterns can be synthesized by controlling the amplitude and phase coefficients of these mode outputs in the same manner that the amplitude and phase coefficients are controlled in a linear array. Experimental data was shown to verify the technique for the instance where multiple beams were desired. Additional experimental data is available in references 1 through 3. These experimental efforts describe the characteristics of a 16-element scanning array designed to provide 18 db sidelobes. A 16-element octave bandwidth array is also described in this reference.

Bibliographies

1. G. G. Chadwick, J. C. Glass, “Investigation of a Multiple Beam Scanning Circular Array,” Scientific Report No. 1, prepared for AFCRL under Contract No. AF19(628)367, AD-411868; 31 December 1962.

2. Radiation Systems, Incorporated Technical Proposal TP-217(U), “Steerable Array Design,” dated 21 September 1964.

3. Radiation Systems, Incorporated Technical Report No. 45, “Multi-Beam Mobile Antenna Array,” prepared for Radio Corporation of America under Contract No. MOB-12-9-1 dated 24 February 1964.

4. T. T. Taylor, “A Synthesis Method for Circular and Cylindrical Antennas Composed of Discrete Elements,” Trans. IRE Antennas and Propagation, No. 3, p. 251; August 1952.

5. Ta-Shing Chu, “On the Use of Uniform Circular Arrays to Obtain Omnidirectional Patterns,” Trans. IRE, Vol. AP-7, pp. 436-438; October 1959

6. J. Blass, “Multidirectional Beam Scanning Antenna Array,” First Interim Report No. W. O. 4071-1, prepared for Rome Air Dev. Center under Contract AF-30(603)1920; July 1958 - April 1959.

7. J. P. Shelton and K. S. Kelleher, “Multiple Beams from Linear Arrays, Trans.” IRE, Vol. AP-9, No. 2, pp. 154-161; March 1961.

8. William P. Delaney, “An RF Multiple Beam Forming Technique,” Massachusetts Institute of Technology, Lincoln Laboratory, Technical Report dated 9 August 1961.

9. J. Butler and R. Lowe, “Beam Forming Matrix Simplifies Design of Electronically Scanned Antennas,” Electronic Design 9, 170; 12 April 1961.

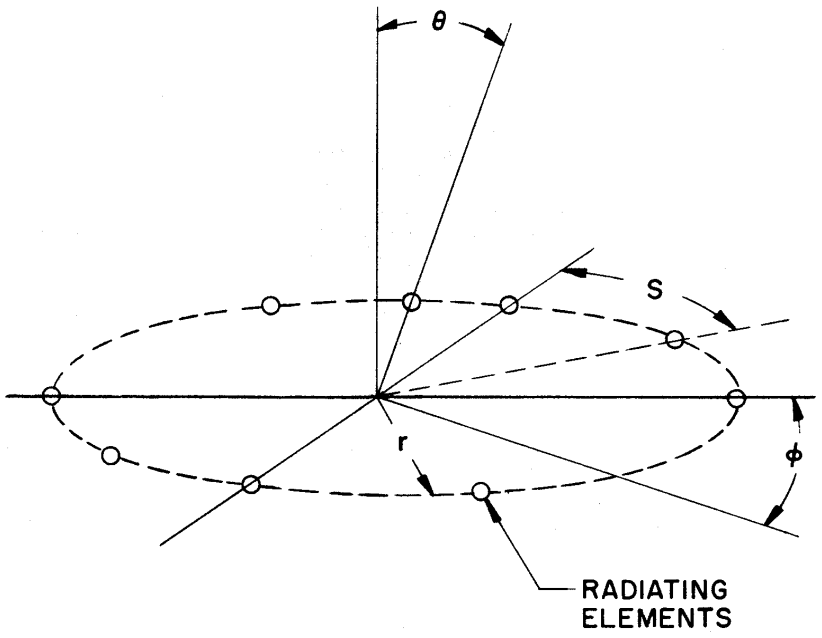

Figure 1. Basic geometry and coordinate system of the cylindrical array.

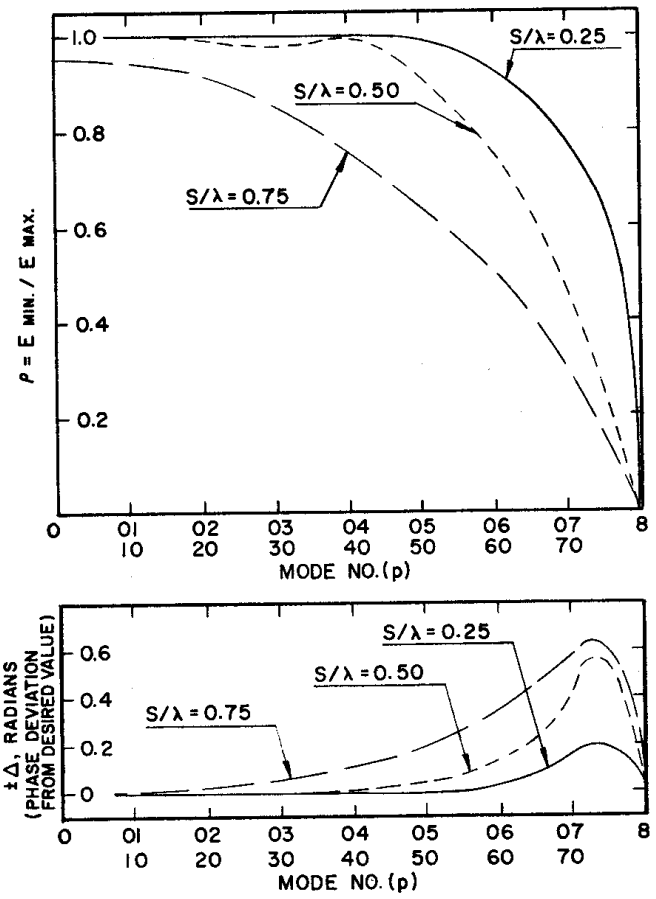

Figure 2. Mode purity in terms of amplitude and phase 16 deviation for an element pattern of the form $\cos^{16} \emptyset$.

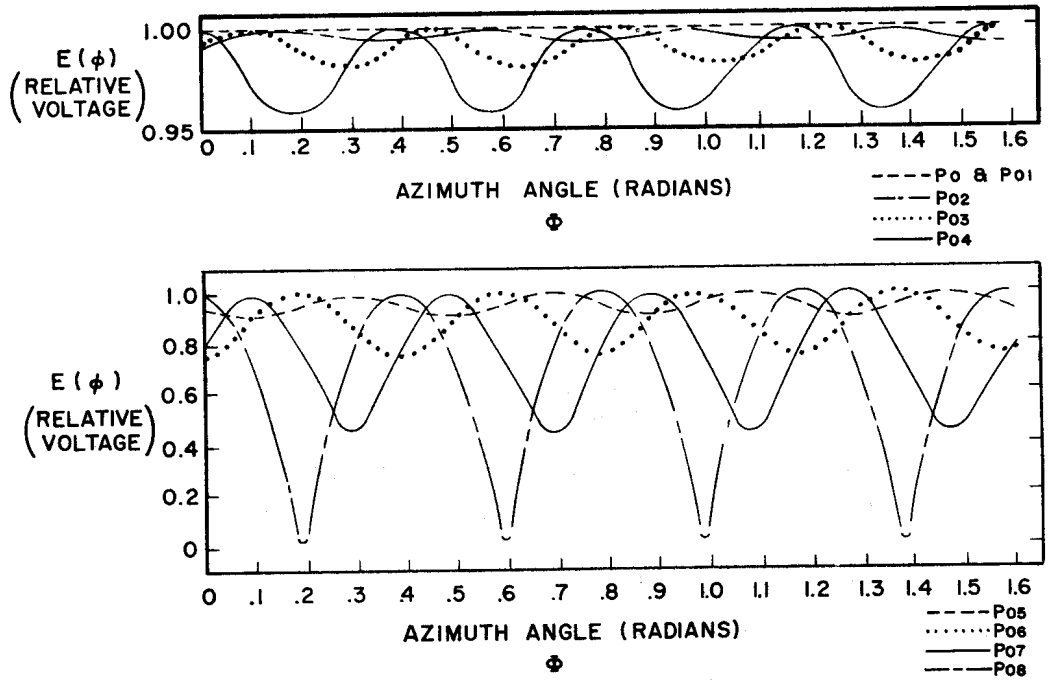

Figure 3. Voltage patterns vs. azimuth angle for element function of Figure 2.

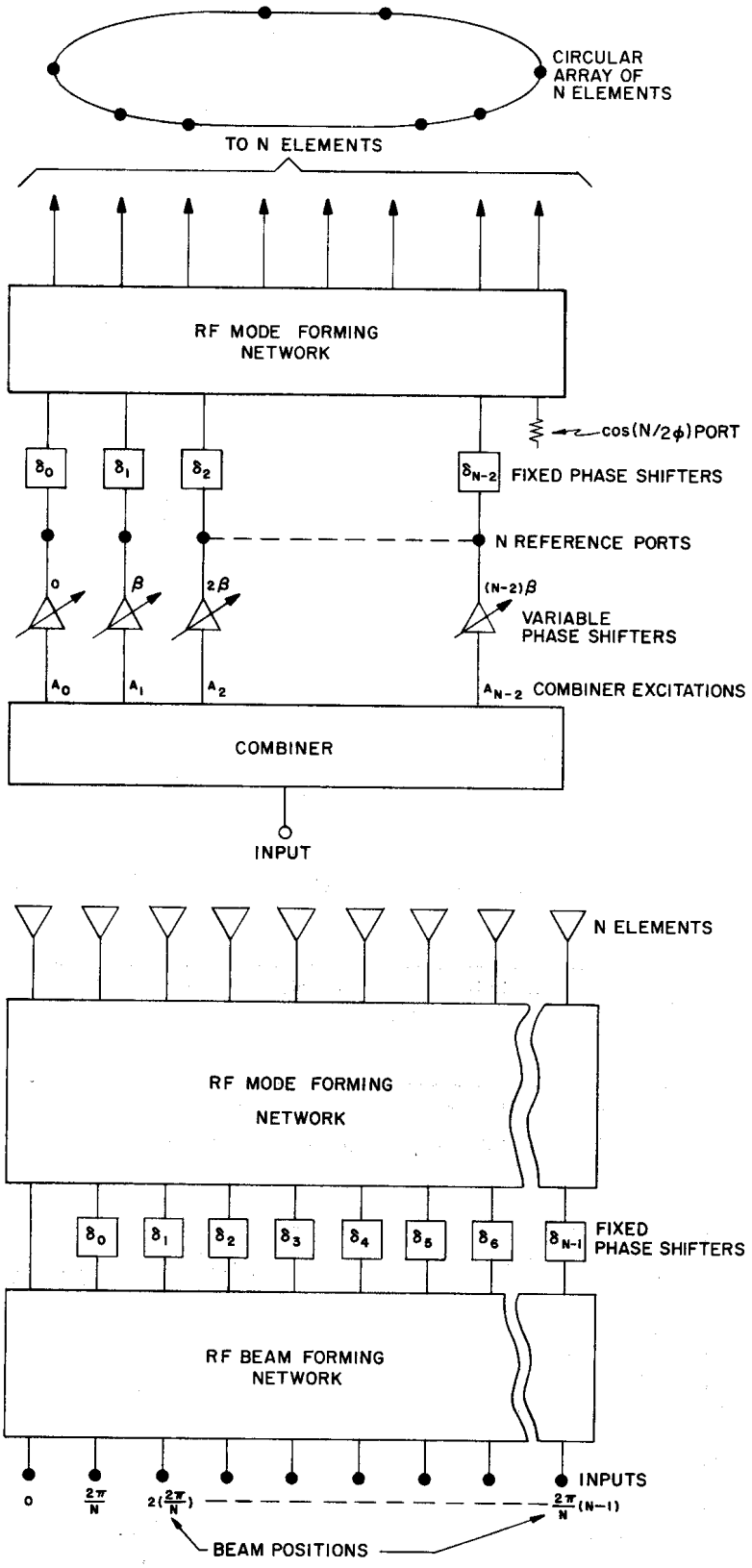

Figure 4. **a) Generalized block diagram of an antenna system with a scanning azimuth beam; b) Generalized block diagram of an N-element multiple-beam circular array.**

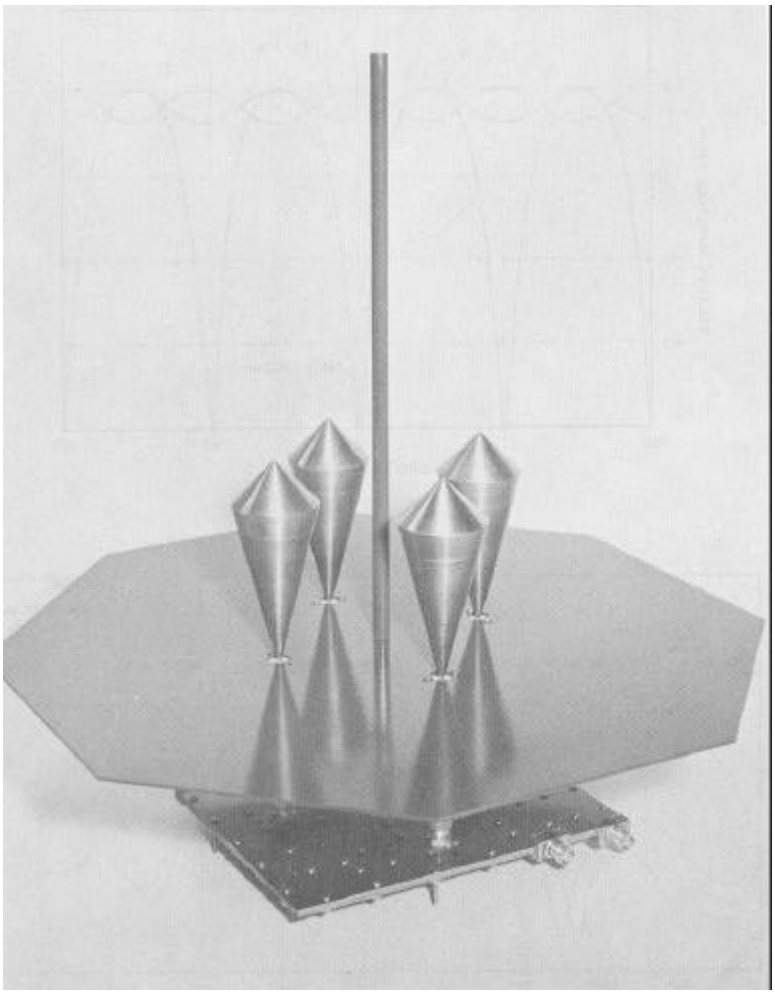

Figure 5. An experimental four-element multiple-beam array.

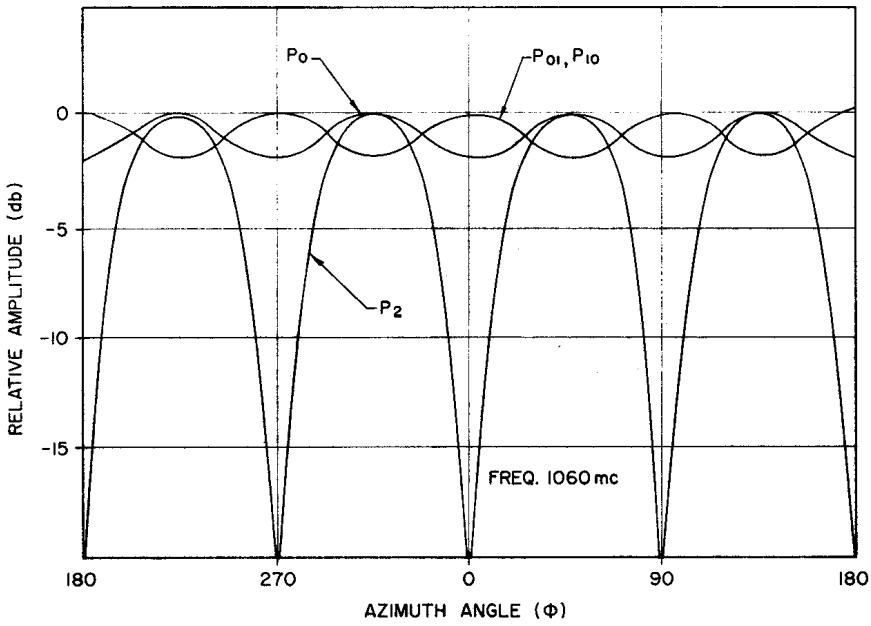

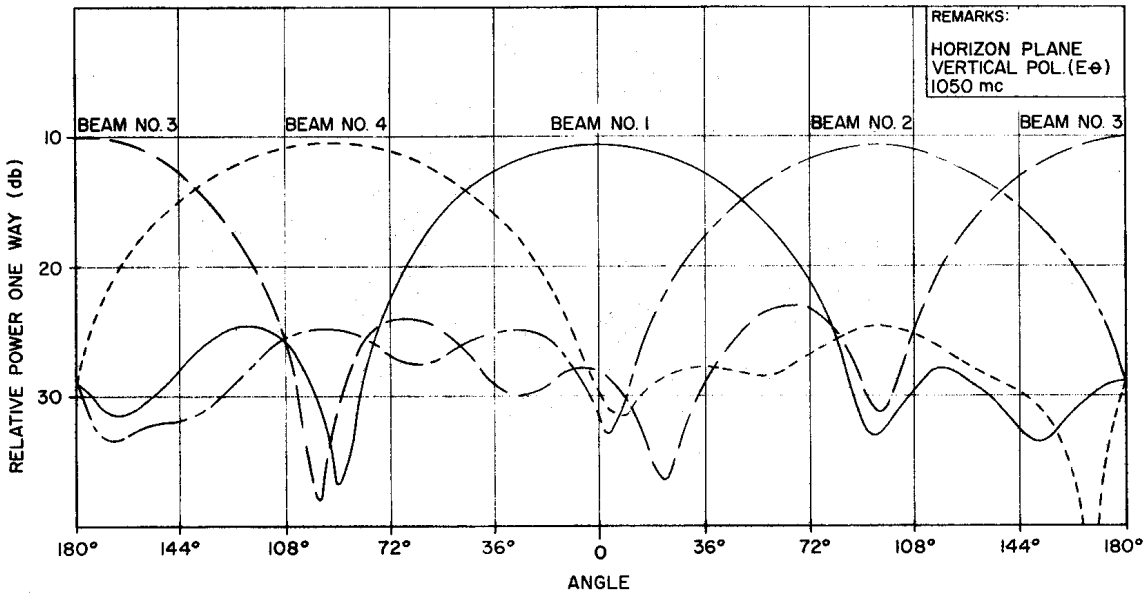

Figure 6. **a) Mode patterns of the monopole array fed by a fourport matrix; b) Beam patterns of the four-element multiple-beam circular array.**

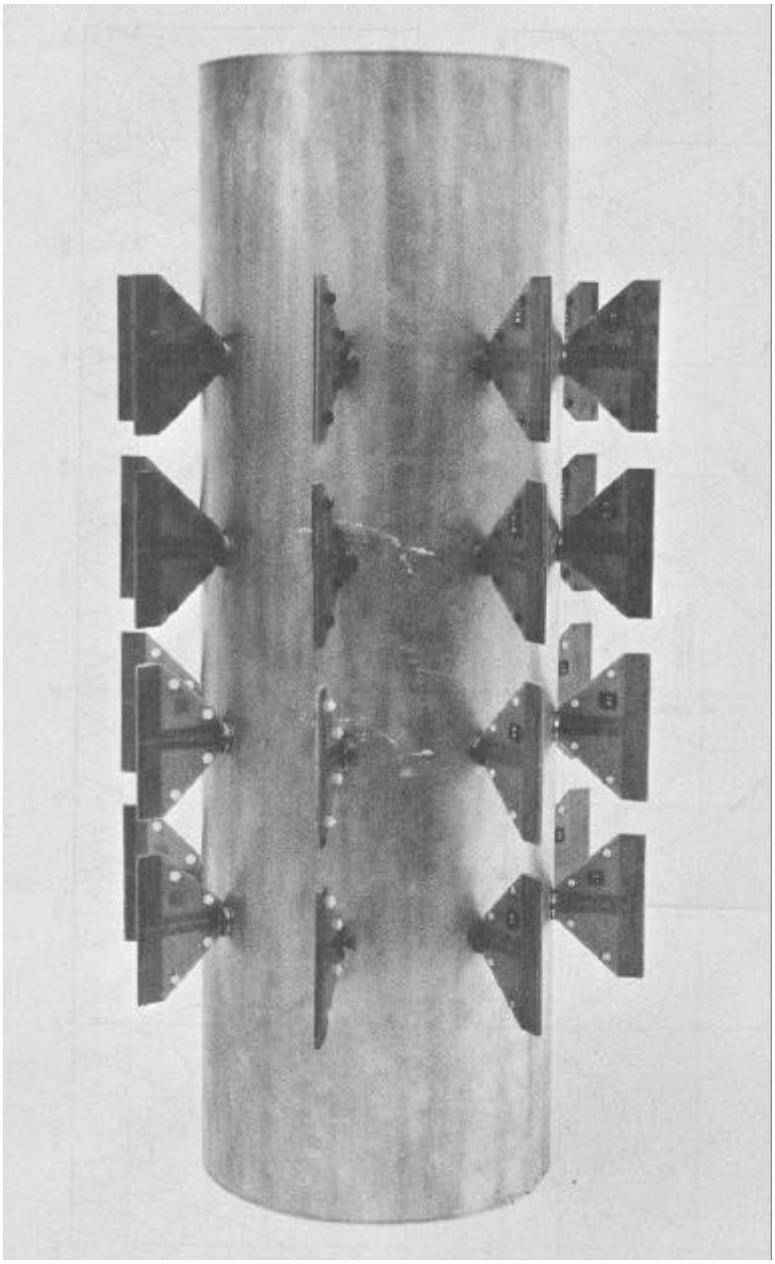

Figure 7. An experimental 4 x 8 multiple-beam cylindrical array.

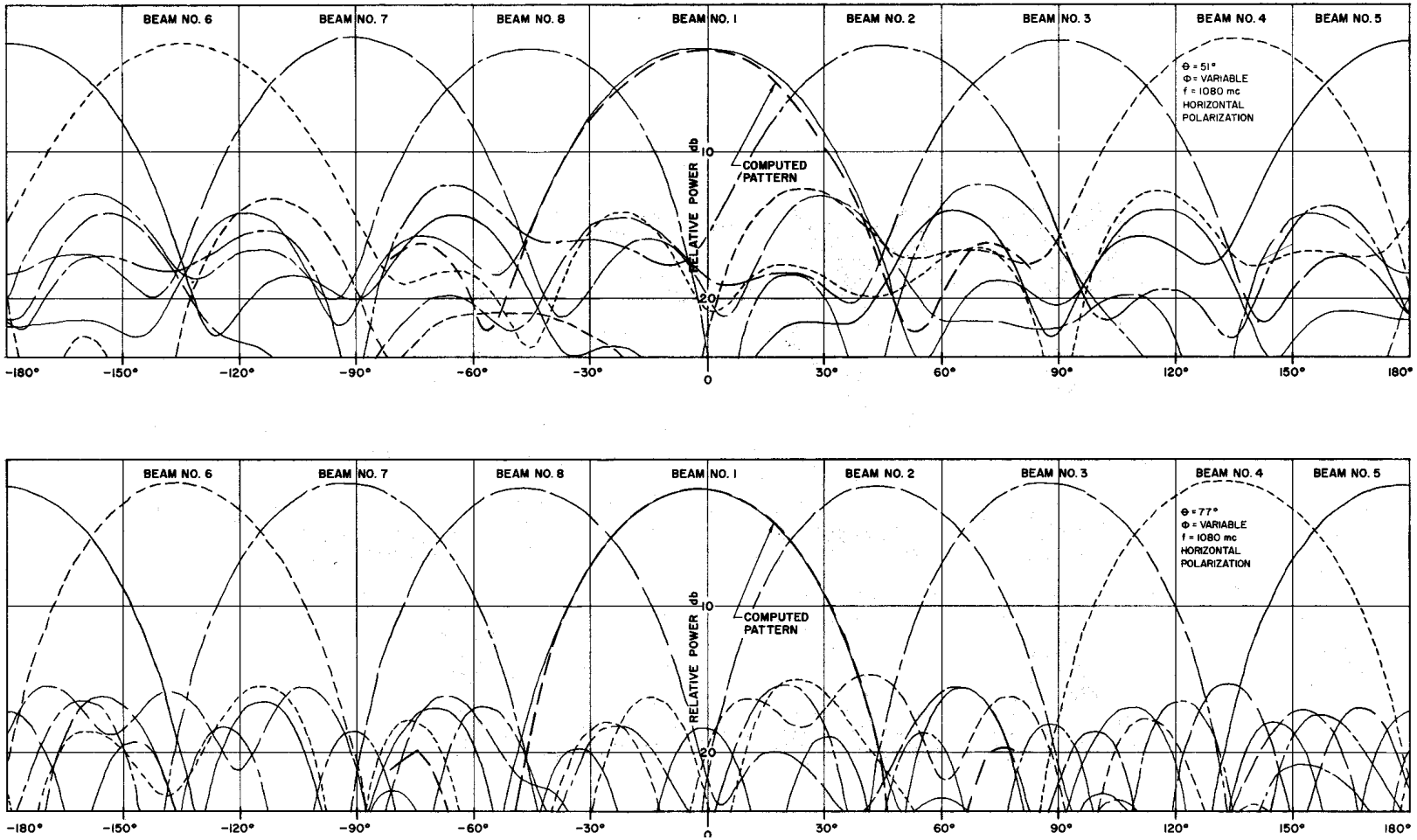

Figure 8. Azimuth plane patterns of the 4 X 8 multiple-beam array at two elevation stations.

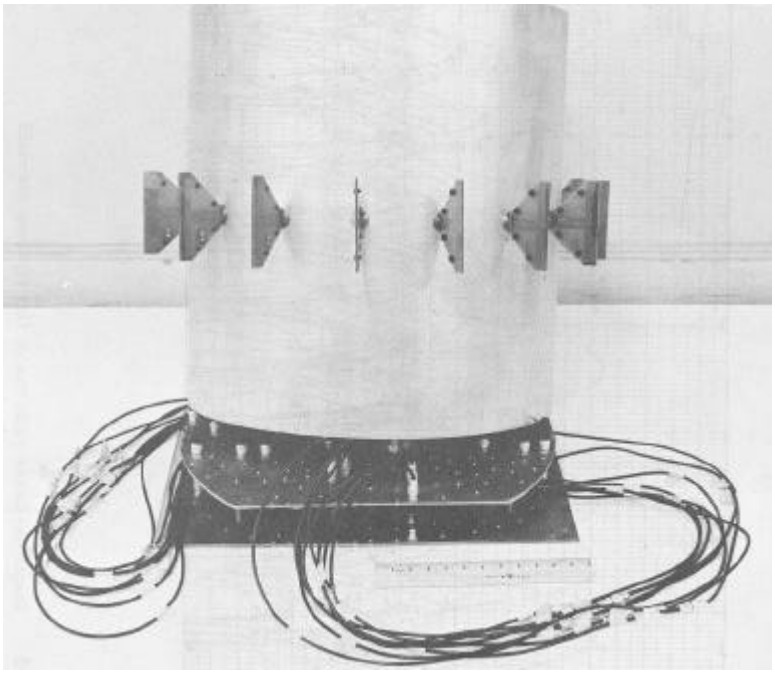

Figure 9. An experimental sixteen-element multiple-beam cylindrical array.

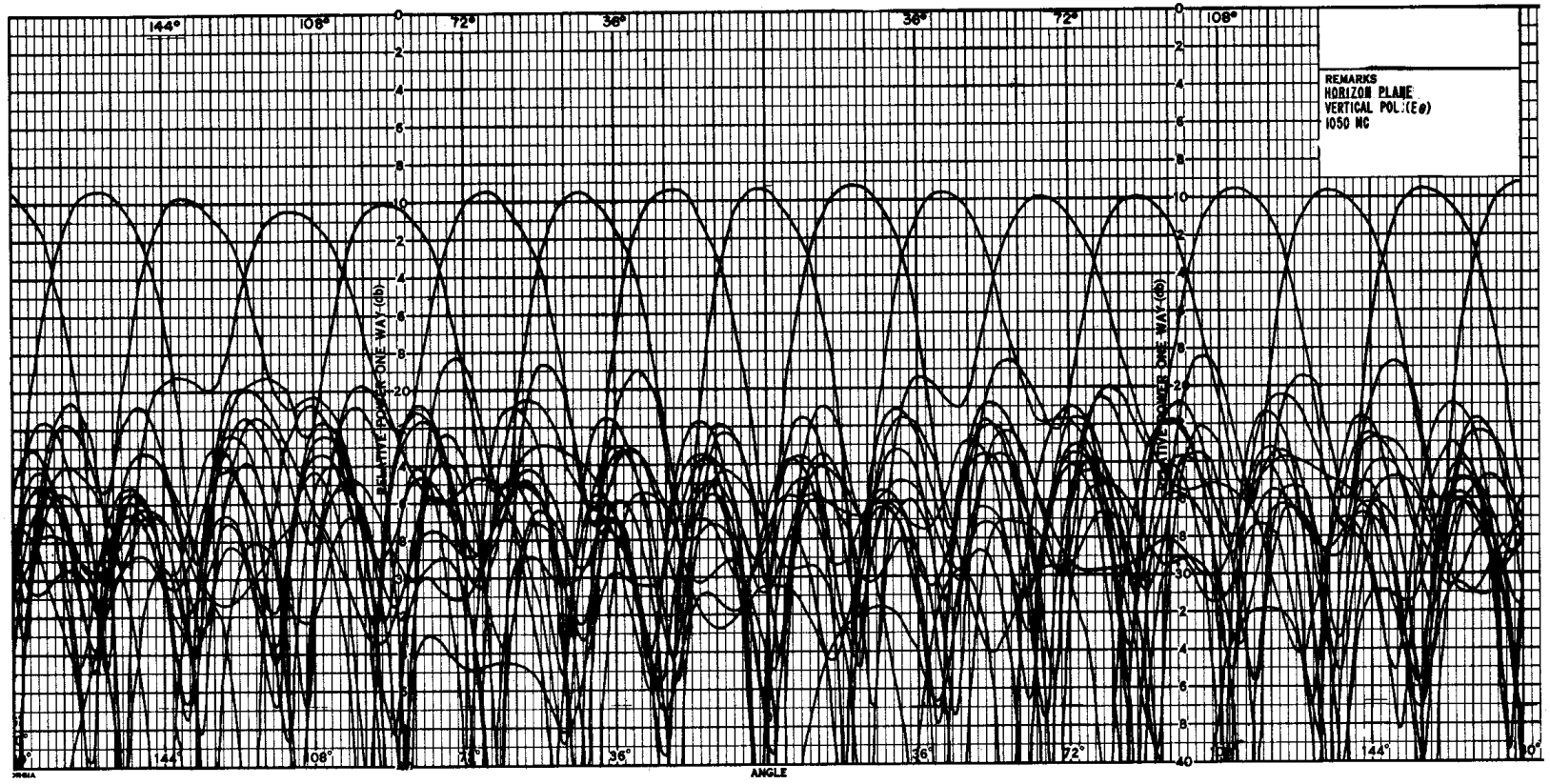

Figure 10. Multiple-beam patterns of the sixteen-element cylindrical array.